International Journal of Thermal Sciences 165 (2021) 106927

Contents lists available at ScienceDirect

International Journal of Thermal Sciences

journal homepage: http://www.elsevier.com/locate/ijts

Influence of nanostructure morphology on the heat transfer and flow characteristics in nanochannel

Shuting Yao [a,b,c], Jiansheng Wang [a,c,*], Xueling Liu [a,c,**]

[a] Key Laboratory of Efficient Utilization of Low and Medium Grade Energy, MOE, School of Mechanical Engineering, Tianjin University, Tianjin, 300350, PR China
[b] College of Petrochemical Technology, Lanzhou University of Technology, Lanzhou, 730050, PR China
[c] Tianjin Key Laboratory of Nonlinear Dynamics and Chaos Control, School of Mechanical Engineering, Tianjin University, Tianjin, 300350, PR China

ARTICLE INFO

Keywords:
Nanochannel
Nanostructure morphology
Heat transfer
Flow resistance
Molecular dynamics

ABSTRACT

Based on the molecular dynamics principle, the convective heat transfer of the fluid through nanochannel with various rough nanostructure morphologies is investigated. The influences of nanostructure free shear ratio, morphology period and nanostructure depth on the flow and heat transfer characteristics are probed. A comprehensive evaluation on the convective heat transfer in rough nanochannel considering the flow resistance is performed. The result shows that the temperature jump and velocity slip dominate the heat and momentum exchange between the channel wall and fluid. Under the weak wall-fluid interaction, the smaller the nanostructure free shear ratio, the better the heat transfer performance as well as drag reduction characteristic. In contrast, the smaller the nanostructure morphology period, the better the heat transfer performance, the greater the flow resistance. Therefore, the wall rough morphology with small free shear ratio and sparse nanostructures is conducive to heat transfer augmentation and drag reduction jointly. The deeper rough nanostructure groove is unfavorable to reduce the flow resistance. The combination of rough nanostructure morphology and weak wall-fluid interaction is crucial, which will bring about a favorable impact on the heat transfer and flow resistance in nanochannel. Specifically, the nanostructure free shear ratio with $\phi_a = 0.1875$ is a favorable rough morphology to obtain optimum heat transfer and drag reduction characteristics in nanochannel.

1. Introduction

With the development of science and technology, miniaturization and nanotechnology have become significant in fields such as natural sciences and engineering technology. Especially, the rapid advancement of micro manufacturing and processing technology has promoted the wide application of micro/nano technology in fields like electronic device thermal management, energy saving, aerospace technology, air conditioning and refrigeration, biomedical detection, information technology and chemical industry [1,2]. Meanwhile, it has also triggered the emergence of some unconventional physical phenomena in micro/nanoscale devices or channels, such as micro/nanoscale flow and heat transfer. Different from the conventional macroscopic scale, the role of surface force in flow and heat transfer at such confined micro/-nanoscale space becomes dominant, which resulted in abnormal flow behavior and thermal phenomenon in the region adjacent to the wall surface [3]. Particularly, the interfacial phenomena such as velocity slip and temperature jump will have a significant effect on the flow behavior and interfacial heat transfer. Since the dimension of system or device is dramatically reduced to the nanoscale, even to the same order of magnitude as the mean free path of fluid molecules, the traditional continuous medium assumption and numerical simulation method will not be applicable. In addition, the experimental investigation on the nanoscale flow and heat transfer is limited and challenging due to the experimental errors and the difficulty of processing and measuring. Based on the first principle, molecular dynamics (MDs) simulation can describe physical process from atomic level, and provide detailed information about fluid microstructure and flow behavior as well as thermal transport properties. Besides, the influence of intermolecular interaction on the flow behavior becomes more obvious with the

* Corresponding author. Key Laboratory of Efficient Utilization of Low and Medium Grade Energy, MOE, School of Mechanical Engineering, Tianjin University, Tianjin, 300350, PR China.
** Corresponding author. Key Laboratory of Efficient Utilization of Low and Medium Grade Energy, MOE, School of Mechanical Engineering, Tianjin University, Tianjin, 300350, PR China.
E-mail addresses: jsw@tju.edu.cn (J. Wang), lxling@tju.edu.cn (X. Liu).

https://doi.org/10.1016/j.ijthermalsci.2021.106927
Received 18 November 2020; Received in revised form 17 February 2021; Accepted 19 February 2021

reduction of system or device dimension. Molecular dynamics method has unique advantages in simulating the interaction between particles. Thus, molecular dynamics has gradually become a powerful tool to study the flow behavior and heat transfer at the nanoscale level [4], and increasing attentions had transferred to use MDs to observe fluid flow behavior and heat transfer feature. In the past few decades, the investigations on the nanoscale heat transfer were conducted sufficiently. It was mainly focusing on two aspects: one was thermal resistance (or temperature jump) and its effect on the interfacial heat transfer [5–8], the other was phase change heat transfer such as boiling heat transfer [4,9,10]. Various studies mentioned above mostly concentrated on pure heat conduction between solid wall and fluid, and no flow of fluid occurred. Yet, as far as fluid flow in nanochannel was concerned, the related researches mainly put emphasis on interfacial velocity slip [11–13] and its influence factors including channel height, surface roughness and interface wettability, etc [14,15] as well as fluid transport properties such as shear viscosity and diffusion coefficient [16–18]. In the vast majority of these studies, the heat exchange between fluid and solid wall was not considered.

Actually, utilizing convective heat transfer in micro/nanoscale channel to cool the electronic or mechanical devices is of utmost importance for guaranteeing the effective operation of the system. However, there are few investigations on the nanoscale convective heat transfer with MDs method. A clear understanding of factors affecting convective heat transfer in nanochannel has significant implications not only in the design of micro/nanofluidic devices but also in their applications. Markvoort et al. [19] firstly simulated the convective heat transfer in nanochannel by exerting driving force on the fluid atoms located in the entrance region and resetting fluid atoms temperature at the inlet. The results showed that wall-fluid interaction strength was an important factor affecting heat transfer characteristics. Based on Markvoort's method, Ge et al. [20] improved this method by changing the order of resetting temperature region and force region. It was found that heat transfer performance enhanced with the augment of the wall-fluid interaction strength. Gu et al. [21] studied convective heat transfer process in nanochannel, and focused on the effect of the axial heat conduction caused by periodic boundary condition on the heat transfer. It has proved that the influence of outlet axial heat conduction on the local fluid temperature gradually decreased with the increase of $\underline{Pe}$ number. Marable et al. [22] studied the effects of wall-fluid interaction, channel height, flow velocity and solid wall temperature on the interfacial temperature jump and heat transfer. Thomas et al. [23] investigated the forced convective heat transfer of argon fluid flowing through carbon nanotubes and carbon nanotube arrays. It has been proved that the wall-fluid interaction strength was the most important influence factors among mentioned above.

Besides, it's found that nanoparticle properties such as particles size and particles morphologies also play a significant role in affecting heat transfer. As a passive control method to achieve thermal conductivity enhancement by adding nanoparticles into the base fluids, nanofluids has also attracted considerable interests [1,24–26]. Philip et al. [27–31] conducted a lot of useful and continuous research work on the thermal conductivity enhancement of various kinds of nanofluids. Especially, the influence mechanism of nanoparticle size, nanoparticle morphology, concentration and aggregating behavior, on the thermal property of nanofluids, was investigated comprehensively. In addition, the relevant developments and applications in nanofluids were better illustrated in review works [1,26,28]. In terms of the effect of nanoparticles on convective heat transfer in nanochannel, Motlagh et al. [32] performed the convective heat transfer of nanofluid flowing through the channel, and found that nanoparticles can facilitate the heat transfer between solid wall and fluid. Furthermore, Motlagh et al. [33] investigated the effects of cylindrical and spherical nanoparticles as well as their aggregation on the nanofluid heat transfer performance. The result indicated that the aggregation of nanoparticles was not conducive to heat transfer between nanofluid and wall.

In addition to the above factors, surface modification is another method to achieve heat transfer enhancement, and extensive efforts have been conducted to explore heat transfer enhancement with surface modification. Especially, the effects of various wall roughness on the boiling heat transfer enhancement were experimentally investigated [34–38]. Apart from the mentioned above on the macroscale, available studies [4,9] have also shown that nanoscale surface roughness, even the roughness with molecular scale, were also quite significant for interfacial phenomenon and greatly influenced heat transfer between fluid and solid wall. In fact, the surface roughness in micro/nano fabricated channels may often be comparable to the mean free path of fluid molecules in practical micro/nanosacle engineering systems [39]. Compared with the relative surface roughness that can be ignored in macroscopic channel, the relative surface roughness in nanochannel becomes very large owing to the remarkable reduction of the system characteristic dimension. Considering that near-wall region is the main domain affected by the wall-fluid interaction, it is obvious that the nanoscale wall roughness will have a significant impact on the interfacial heat transfer in nanochannel. Chakraborty et al. [40] probed the role of surface modification in convective heat transfer in nanochannel. The results showed that surface roughness could dramatically enhance the heat transfer between fluid and solid wall. Motlagh et al. [33,41] pointed out that wall roughness played a significant role in boosting the heat transfer performance. Besides, Wang et al. [42] investigated the influences of wall properties on temperature jump and Nusselt number in the process of nanoscale convective heat transfer. It observed that a special selected coating wall could play a role of thermal bridge between channel wall and fluid, which will bring about a remarkable enhancement of convective heat transfer. In summary, the convective heat transfer in nanochannel is affected by many factors, including wall-fluid interaction strength, surface roughness or surface coating, nanoparticles, wall material properties, etc.

It is worth mentioning that a rather high pressure drop occurs in nanoscale channels or devices owing to a very small hydraulic diameter, compared with those in conventional macroscale channels. From the perspective of energy saving and consumption reduction, it is desirable to maintain a lower flow resistance while transferring as much heat as possible between fluid and channel wall in many engineering applications. However, up to now, the flow resistance during the convective heat transfer in nanochannel has been paid less attention. Although many investigations on the factors affecting the convective heat transfer have been conducted, the influence of these factors on the flow resistance is unclear. In this context, it is necessary to pay attention to flow resistance while achieving the heat transfer enhancement in nanochannel.

How to reduce flow resistance in nanochannel? The investigations on drag reduction in microchannel flow have shown that the hydrophobic surface was conducive to drag reduction because of the larger velocity slip [43,44]. Moreover, the drag reduction feature was also closely related to surface microstructure such as spacing and shape [45–47], and the rough superhydrophobic surface has better drag reduction characteristic than that of rough hydrophilic surface does. Thus, the wall hydrophobic property and surface microstructure have a favorable effect on the drag reduction in microchannel flow. Yet, how does rough nanostructure influence the flow resistance in nanochannel flow? Whether the effective combination of surface hydrophobicity and rough nanostructure is likely to obtain more effective drag reduction and enhance heat transfer jointly or not? So far, the role of rough nanostructure morphology and wall-fluid interaction in velocity slip and flow resistance in nanochannel is still ambiguous, which is yet to be adequately resolved. A comprehensive evaluation about convective heat transfer in nanochannel needs to be probed in depth.

In present work, the nanoscale convective heat transfer under the consideration of the flow resistance is performed with molecular dynamics. The influences of rough nanostructure morphologies and wall-fluid interaction on the flow resistance and heat transfer

characteristics are investigated. Under the condition of weak wall-fluid interaction, the effects of rough nanostructure morphology on the velocity slip and flow resistance are analyzed. The variations of temperature jump and Nusselt number with rough nanostructure morphology are discussed as well. The influence mechanism of wall-fluid interaction and rough morphology on the heat and momentum transfer in nanochannel is further revealed. Furthermore, an optimum rough nanostructure morphology is discussed.

2. Theoretical analysis

2.1. Flow governing equations

When viscous fluid flows through a rectangle channel, the velocity along the x-direction can be determined by the Navier Stokes equation as:

$$\rho u_x \frac{\partial u_x}{\partial x} = -\frac{\partial p}{\partial x} + \mu \frac{\partial^2 u_x}{\partial z^2} \tag{1}$$

If fluid velocity does not vary along the x-direction, Eq. (1) can be simplified to:

$$\mu \frac{\partial^2 u_x}{\partial z^2} = \frac{\partial p}{\partial x} \tag{2}$$

where ρ is fluid density, μ is fluid shear viscosity.u_x is fluid streamwise velocity, $\frac{\partial p}{\partial x}$ is pressure gradient in x direction. Generally, the slip length L_s can be obtained by extrapolating the velocity profile of fluid, which is given by:

$$L_s = \frac{u_s}{\left.\frac{\partial u_x}{\partial z}\right|_{z=w}} \tag{3}$$

where u_s is the slip velocity at the wall-fluid interface.$\left.\frac{\partial u_x}{\partial z}\right|_{z=w}$ is fluid velocity gradient at the wall-fluid interface.

The resistance coefficient f can be defined as:

$$f = \frac{\frac{\Delta p}{L_x} D_h}{\frac{1}{2}\rho {u_m}^2} \tag{4}$$

where $\frac{\Delta p}{L_x}$ is the pressure gradient along the x direction. D_h is hydraulic diameter, for smooth channel, $D_\mathrm{h} = 2H$. For rough channel, $D_\mathrm{h} = 2H+2h$. u_m is average velocity of the fluid in channel. When the fluid flows through the nanochannel, the flow is driven by applying an external force F_ext to each of the N fluid atoms in x direction. Thus,$NF_{ext} \rightarrow (\Delta p)A$ (N is the number of fluid atoms,A is the channel cross section area), Eq. (4) can be written as:

$$f = \frac{F_{ext} D_h}{\frac{1}{2} m u_m^2} \tag{5}$$

where m is the mass of fluid atom. In present work, the pressure difference (i.e. the external force) is constant, while the channel hydraulic diameter and the average velocity of the fluid in channel are different in smooth and rough channel. For better comparison, taking the resistance coefficient of the smooth channel with the strong wall-fluid interaction as a reference, which is denoted as f_0, then, the relative resistance coefficient f^* is defined as:

$$f^* = \frac{f}{f_0} \tag{6}$$

In addition, the surface friction coefficient can be calculated as following:

$$c_f = \frac{\mu \left.\frac{\partial u_x}{\partial z}\right|_{z=w}}{\frac{1}{2}\rho {u_m}^2} \tag{7}$$

Similarly, the surface friction coefficient of the smooth channel with strong wall-fluid interaction is defined as c_{f0}, and the relative surface friction coefficient is defined as following:

$$c_f^* = \frac{c_f}{c_{f0}} \tag{8}$$

2.2. Basic equations of heat transfer

For convective heat transfer, the local mean temperature $T_m(x)$ of the fluid in the cross-section at different x position is defined as Eq. (9). The local heat transfer coefficient $h(x)$ can be obtained by Eq. (10), and the local Nusselt number Nu_x can be calculated with Eq. (11). To avoid the influence of the variation in thermal conductivity derived from the wall-fluid interaction on the local heat transfer coefficient, the local Nusselt number can be obtained from Eq. (12) by combining Eq. (10) and Eq. (11):

$$T_m(x) = \frac{\int_0^H c\rho u_x(x,z) T(x,z) dz}{\int_0^H c\rho u_x(x,z) dz} \tag{9}$$

$$h(x) = \frac{\lambda}{(T_m(x) - T_\mathrm{w})} \left.\frac{\partial T}{\partial z}\right|_{z=w} \tag{10}$$

$$Nu_x = \frac{h(x) D_h}{\lambda} \tag{11}$$

$$Nu_x = \frac{D_h}{(T_m(x) - Tw)} \left.\frac{\partial T}{\partial z}\right|_{z=w} \tag{12}$$

where c is specific heat capacity of the fluid, $T(x,z)$ is temperature of the fluid along the x-direction. λ is thermal conductivity of the fluid,T_w is wall temperature. $\left.\frac{\partial T}{\partial z}\right|_{z=w}$ is temperature gradient at the wall-fluid interface. Similar to the slip length, the temperature jump length L_k can also be defined by extrapolating the temperature profile of the fluid from mainstream region into the solid wall, where wall temperature reaches.

$$L_k = \frac{\Delta T}{\left.\frac{\partial T}{\partial z}\right|_{z=w}} \tag{13}$$

Here, ΔT is the temperature jump at the wall-fluid interface.

3. Numerical process and potential models

3.1. Simulation details

The computational domain is shown in Fig. 1 (a). The upper and lower solid wall are composed of platinum atoms with a thickness of $D =$ 24 Å. The wall atoms are arranged following the FCC type unit. The channel size is 412 × 80 × 120 Å^3 and the distance separated by the upper and lower solid wall (channel height) is H = 120 Å. The nanochannel would be filled with argon atoms and the fluid density of 1200 kg/m^3 is achieved. In order to effectively observe the convective heat transfer between the solid wall and fluid, the Langevin thermostat is used to keep the upper and lower solid wall at the specified temperature T_w = 200K. While the fluid domain is divided into three independent regions shown in Fig. 1 (a): force region, thermostat region and sample collection region. The force region is applied to the x-directional coordinates of −12.0 Å$<x<$ −8.0 Å. A constant driving force of 3.4 pN is imposed to the fluid atoms located in force region. Then, temperature resetting is performed for fluid atoms inside the region of −8.0 Å$<x<$ 0

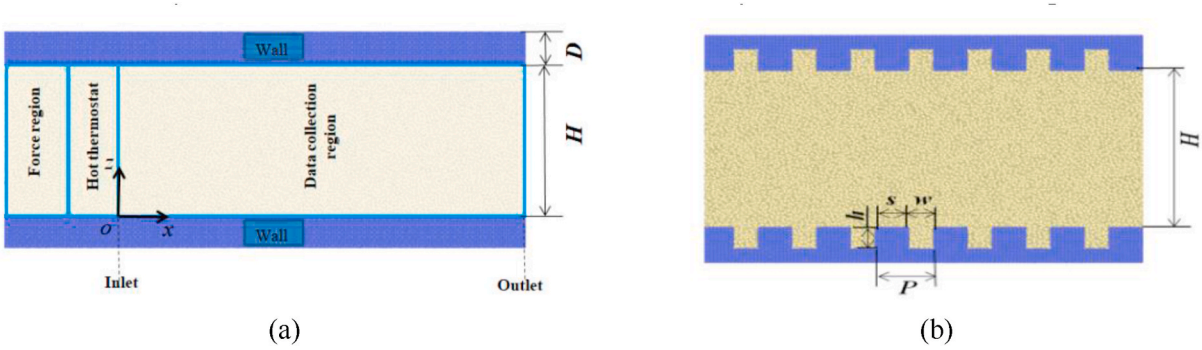

Fig. 1. Schematic model of convective heat transfer in nanochannel.

Å without disturbing the directional flow, and the fluid is controlled to be in supercritical state to avoid phase transition [20]. After temperature resetting, a specified initial temperature $T_{int} = 300K$ is generated at the inlet. Then, a process of convective heat transfer in parallel-plate nanochannel with constant wall temperature can be explored in region of 0 Å$<x<$ 400 Å.

Besides, periodic boundary conditions are applied in the *x*- and *y*-directions, respectively. All simulation cases are performed with a timestep of 1fs. The Newton's equations of motion are integrated by the Velocity-Verlet algorithm. In addition, the entire simulation domain is relaxed in canonical (NVT) ensemble at 200K for 1.0ns firstly, and then the 0.5ns is used to reach the steady state with an external driving force in the NVE ensemble. After that, the following another 7.5ns is used for sampling, averaging and data collection. An open source molecular dynamics code, LAMMPS is utilized to carry out all simulations in present work [48].

Fig. 1 (b) shows the rough nanostructure with rectangular grooves. As shown in Fig. 1(b), w is the groove width, h is the groove depth and s is the groove spacing. The rough nanostructure free shear ratio is defined as:$\phi_a = \frac{w}{w+s}$, the rough morphology period is defined as: $P = w+s$. A series of nanostructure dimensions under various nanostructure free shear ratios and morphology periods are listed in Table 1 and Table 2, respectively.

3.2. Potential models

The Lennard-Jones (LJ) 12-6 potential model,$\varphi(r_{ij}) = 4\varepsilon\left[\left(\frac{\sigma}{r_{ij}}\right)^{12} - \left(\frac{\sigma}{r_{ij}}\right)^{6}\right], r \prec r_c$ is used to describe the interaction between the atoms. Where i, j corresponds to interacting atoms, respectively. ε is energy parameter and σ is length scale for LJ potential function. r_c is cutoff radius, Å. For the fluid-fluid interaction, $\varepsilon_l = \varepsilon_{ArAr} = 1.67 \times 10^{-21}$J and $\sigma_l = \sigma_{ArAr} = 3.405$ Å. $m_l = m_{Ar} = 6.63 \times 10^{-26}$kg. For atomic interactions between wall atoms: $\varepsilon_s = \varepsilon_{PtPt} = 8.35 \times 10^{-20}$J and $\sigma_s = \sigma_{PtPt} = 2.475$ Å. $m_s = m_{Pt} = 3.24 \times 10^{-25}$kg. For the wall-fluid interaction, according to the Lorenthz-Berthelot rule, the length scale σ_{sl} is given by: $\sigma_{sl} = 2.94$ Å [49,50]. In present investigation, the wall-fluid interaction strength ε_{sl} is set as $1.0\varepsilon_l$ and $0.25\varepsilon_l$, which characterizes the strong and weak wall-fluid interaction [51,52], respectively. Considering the surface wettability can be reflected by the interaction potential between wall and fluid atoms [52–54], so the weak wall-fluid interaction strength characterizes that wall surface is more difficult to be wetted, while the wall surface with the strong wall-fluid interaction strength is more wettable.

Table 1
Nanostructure dimension parameters under different free shear ratios.

Nanostructure depth $h = 4$ Å					Nanostructure depth $h = 16$ Å				
φ_a	w (Å)	s (Å)	h (Å)	P (Å)	φ_a	w (Å)	s (Å)	h (Å)	P (Å)
0.1875	6	26	4	32	0.1875	6	26	16	32
0.25	8	24	4		0.25	8	24	16	
0.375	12	20	4		0.375	12	20	16	
0.5	16	16	4		0.5	16	16	16	
0.75	24	8	4		0.75	24	8	16	

Table 2
Nanostructure dimension parameters under different morphology periods.

Nanostructure depth $h = 4$ Å					Nanostructure depth $h = 16$ Å				
P(Å)	w (Å)	s (Å)	h (Å)	φ_a	P(Å)	w (Å)	s (Å)	h (Å)	φ_a
12	6	6	4	0.5	12	6	6	16	0.5
16	8	8	4		16	8	8	16	
24	12	12	4		24	12	12	16	
32	16	16	4		32	16	16	16	
48	24	24	4		48	24	24	16	

4. Results and discussions

4.1. Verification

According to previous investigations in the fields of convective heat transfer in nanochannel, simulation of convective heat transfer in rough nanochannel considering the flow resistance has not been done so far. In order to verify the results obtained in present work, the convective heat transfer in smooth nanochannel with a size of 400 × 120 × 60 Å^3 is simulated and compared with the results of Ge et al. [20]. In this case, the wall atoms are connected to FCC lattice sites by using harmonic springs with a spring constant of 70 N/m, and the wall-fluid interaction strength is set as $\varepsilon_{sl} = 1.67 \times 10^{-21}$J, which characterizes the normal interfacial wettability. The variation of local Nusselt number along the channel is compared with the results of Ge et al. [20]. As shown in Fig. 2, the local Nusselt number obtained in present work is almost consistent with those obtained in Ref. [20], which indicates that present results are accurate and reliable. In the following sections, the heat transfer and flow characteristics in rough channels with various nanostructure morphologies will be discussed.

4.2. Velocity and temperature distributions

The variations of velocity profiles along the channel height at different x locations in smooth channel and rough channel ($\varphi_a = 0.5$) are shown in Fig. 3. It's found that the fluid velocity along the x direction is almost constant, which indicates that the fluid flow is fully developed. Owing to the lower viscous friction of the channel wall, the maximum velocity of the fluid in mainstream region of smooth channel with the weak wall-fluid interaction is about 100 m/s, which is greater than the maximum velocity of 85 m/s in mainstream region of smooth channel with the strong wall-fluid interaction. It is obvious that the strong wall-

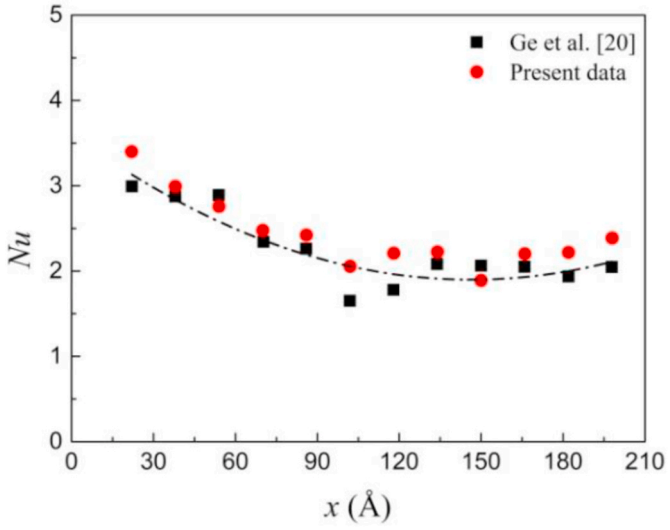

Fig. 2. Variation of Nusselt number along the channel.

fluid interaction reduces the fluid velocity in nanochannel, which is unfavorable for the velocity slip at the wall-fluid interface. By comparing Fig. 3(c) and (d), at the same cross section along the x direction of channels, it's found that average velocity of fluid in rough channel corresponding to the nanostructure depth of 16 Å is lower than that in rough channel corresponding to nanostructure depth of 4 Å. The augment of rectangular nanostructure depth makes more fluid atoms enter the grooves and further hinders the movement of these fluid atoms along the x direction, which results in the decrease of fluid velocity adjacent to the rough wall. And, the velocity in mainstream region also decreases due to the existence of viscous friction between the fluid layers. As a result, the average velocity of fluid in rough channel with large nanostructure depth decreases. In addition, it can be observed that the slip velocity at the wall-fluid interface is greater under the weak wall-fluid interaction strength. Moreover, under the weak wall-fluid interaction, the fluid velocity in rough channel with small nanostructure depth is greater than that in rough channel with large nanostructure depth at the same cross section of channel. So, the slip velocity in rough channel with small nanostructure depth is greater and more obvious by comparing inset in Fig. 3(c) and inset in Fig. 3 (d). Actually, this flow behavior arises from interaction strength between fluid atoms and wall atoms, which is determined by attraction and repulsion forces of wall-fluid atoms as well as interaction contact area between fluid and channel wall. The larger the nanostructure depth, the weaker the tendency of fluid molecules to escape from the grooves, and the weaker the velocity slip.

Under the condition of the weak wall-fluid interaction, the effect of nanostructure depth on the streamlines of fluid in rough channel is depicted in Fig. 4. Here, taking the rough channel with nanostructure shear free ratio of $\varphi_a = 0.5$ as an example. It can be seen clearly that the streamlines near rough wall deforms obviously. There is no macroscopic velocity in nanostructure grooves along the flow direction. As the nanostructure depth increases from 4 Å to 16 Å, the streamline deformation near the rough wall becomes more obvious, indicating that the

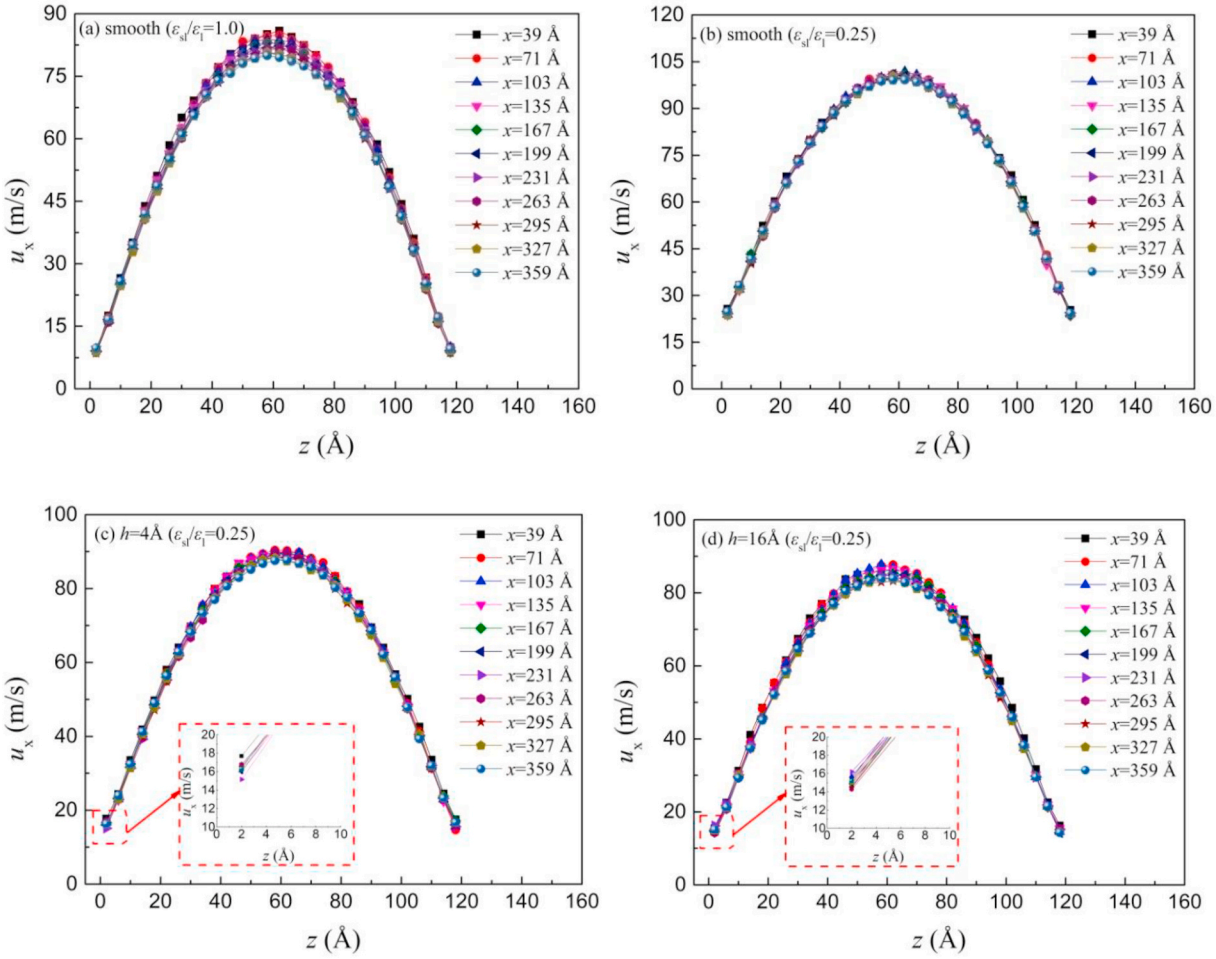

Fig. 3. Velocity profiles at different channel length positions.

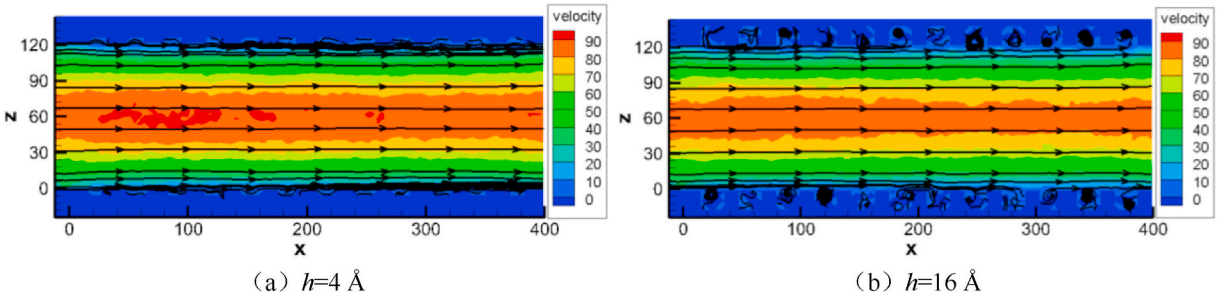

Fig. 4. Streamlines of fluid in rough nanochannel under the different nanostructure depths.

obstruction of rough nanostructure to the movement of fluid atoms is more dramatical. Thus, the more obvious distortion of the streamlines near the wall is demonstrated to be responsible for the lower average velocity of the fluid in rough channel with the larger nanostructure depth.

In the case of strong and weak wall-fluid interaction, the density profiles in channel are illustrated in Fig. 5, which is used to manifest the physical aggregation of fluid atoms near the wall under different nanostructure depths. Similarly, the rough channel with nanostructure shear free ratio of $\varphi_a = 0.5$ is also taken as an example. Compared with the smooth channel, the fluid density distribution in rough channel presents two oscillation stages. In the vicinity of the channel wall, the oscillation degree of density gradually decreases with the increase of the nanostructure depth. Within the nanostructure grooves, the density distribution exhibits secondary oscillation with small amplitude, and the oscillation degree increases with the augment of the nanostructure depth. The variations both in oscillation degree and maximum value of the density outside the nanostructure grooves are similar to the results of Asproulis et al. [55]. It's found that the first peak of density profile in grooves is the maximum, which reflects the amount of fluid atoms closest to the grooves surface is the largest. Meanwhile, the first peak will move toward the grooves surface as the nanostructure depth increases, which demonstrates that more fluid atoms are confined in these grooves due to the attraction force between wall atoms and fluid atoms. Owing to the limitation of nanostructure grooves, the motion of fluid atoms near rough wall is hindered. In addition to the effect of wall rough nanostructures on the density distribution, Fig. 5 also shows that the density distribution near the wall under strong wall-fluid interaction has a greater amplitude with the same wall morphology. It indicates that more fluid atoms are adsorbed near the wall surface, and the movement of fluid atoms along the flow direction is impeded. As a result, it has a lower average velocity of the fluid in channel with the strong wall-fluid interaction and rough nanostructure morphology, just as shown in Fig. 3. Therefore, the density distributions near the channel wall further evidences that the movement of fluid atoms depends on the wall-fluid interaction and nanostructure confinement.

Fig. 6 shows the fluid temperature distributions in smooth and rough channels ($\varphi_a = 0.5$). Compared with the fluid velocity distribution, the variation of fluid temperature along the flow direction has experienced a non-uniform process. When fluid flows along the channel, the average temperature of the fluid decreases gradually along the flow direction due to the cooling effect of the cold channel wall. After the thermal development stage, the flow finally reaches the state of thermal-fully development. Moreover, the temperature profiles are almost overlapping and invariable at the thermal-fully development state in both smooth and rough channel, which is consistent with the thermal development of channel at the macroscale. As shown in Fig. 6, when the fluid flow is thermal-fully developed, the fluid temperature in channel with the strong wall-fluid interaction strength is lower, which indicates that the intensity of convective heat transfer in this case is more sufficient. Compared Fig. 6(c) and (d), it can be found that the fluid in rough channel with the larger nanostructure depth has a lower average temperature at the same channel cross section, which verifies that the intensity of convective heat transfer in channel with the larger nanostructure depth is also higher. According to the definition of temperature jump as expressed in Eq. (13), a greater temperature jump can be observed in rough channel with small nanostructure depth, while the relatively small temperature jump is found in rough channel with the large nanostructure depth. As mentioned above, more fluid atoms will enter into the grooves as the nanostructure depth increases, which results in more frequent atom collisions as well as stronger momentum exchange between fluid and wall atoms. Consequently, the heat transfer enhancement in nanochannel is achieved.

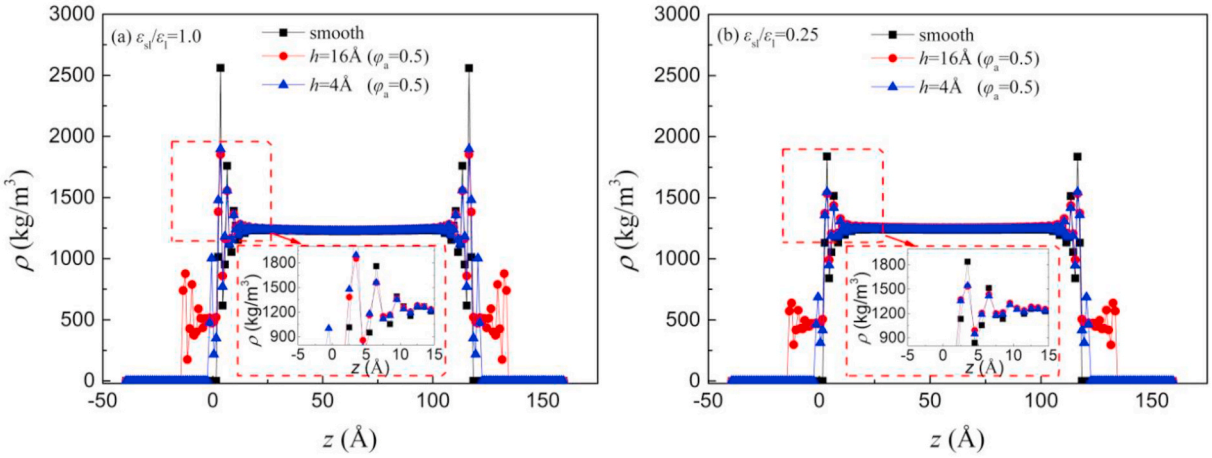

Fig. 5. Density distributions along the channel height.

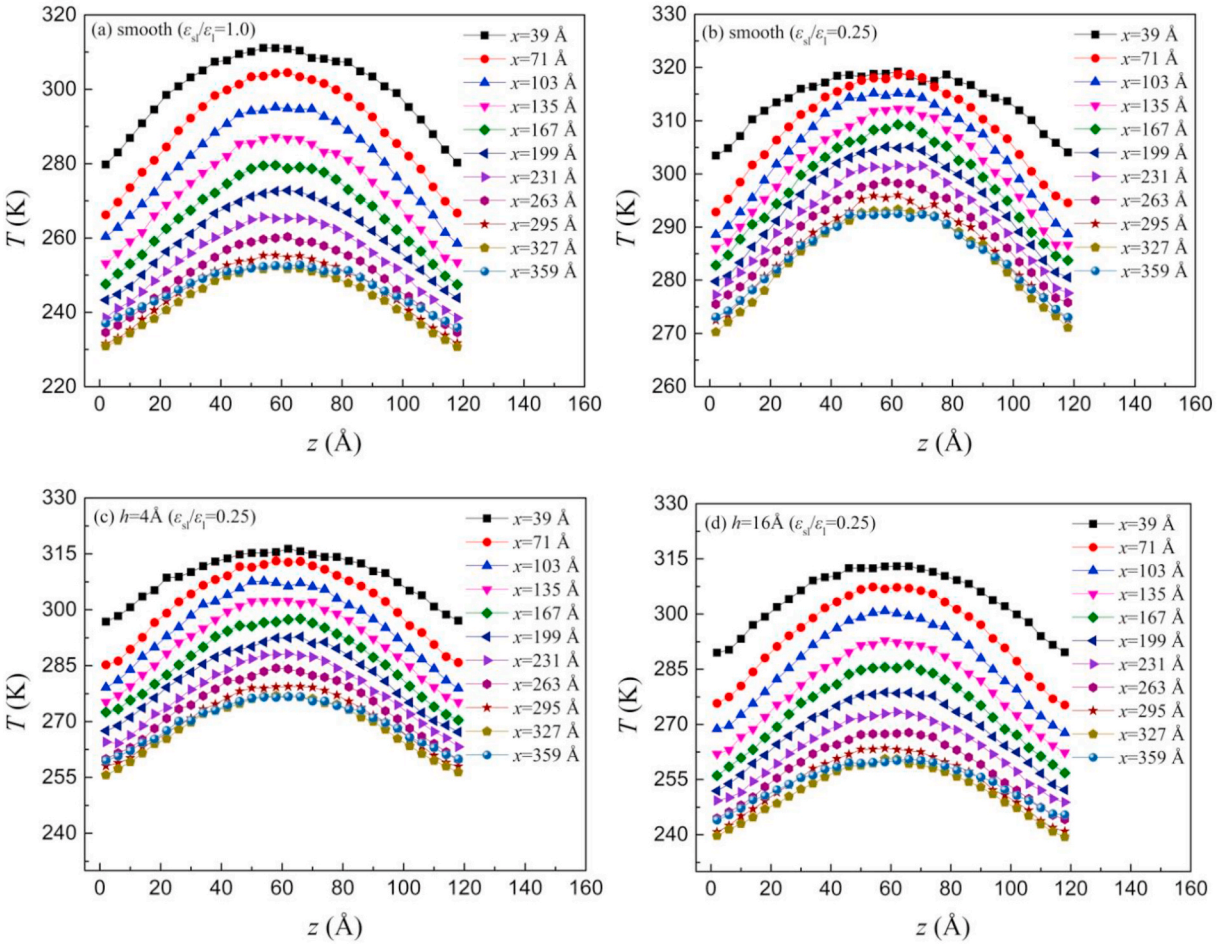

Fig. 6. Temperature profiles at different channel length positions.

4.3. Variation of local flow characteristics

The following content will put emphasis on analyzing flow and heat transfer characteristics from the perspective of the weak wall-fluid interaction strength. The influences of nanostructure free shear ratio and nanostructure morphology period on the density distribution in channel are exhibited in Fig. 7. Here, the nanostructure depth is considered as h = 16 Å. Under the condition of the weak wall-fluid interaction, as shown in Fig. 7(a), the oscillation peak of density near rough wall decreases, while the secondary oscillation peak of the density inside grooves increases gradually with the augment of nanostructure free shear ratio from 0.1875 to 0.75. The fluid atoms attracted in the grooves increase significantly due to the increase of nanostructure width, which makes the secondary oscillation peak of the density increase. Yet, the fluid density in mainstream region of the channel is basically invariable. In comparison, with the increase of the nanostructure morphology period from 12 to 48, the oscillation peak of the density near the rough wall shows a decreasing trend while the

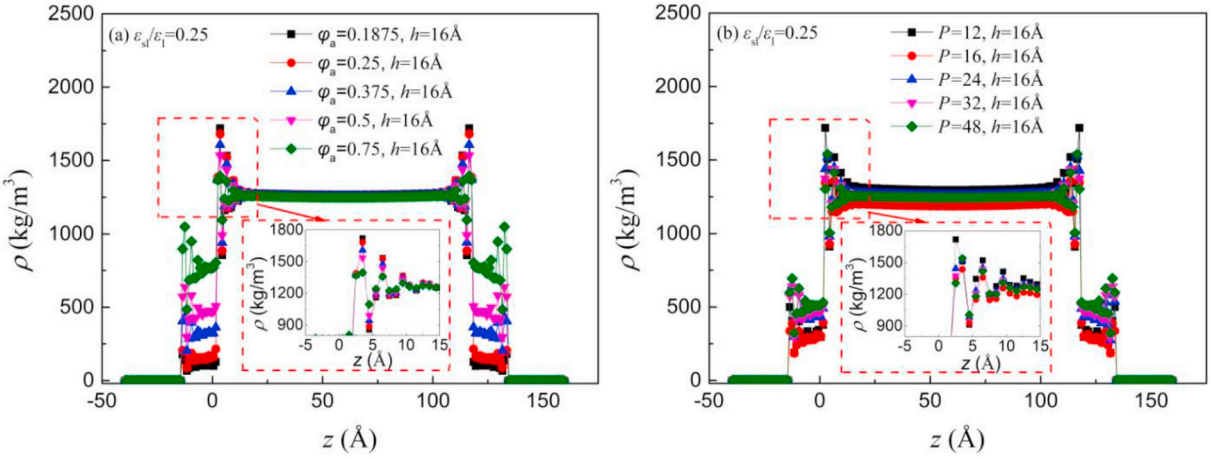

Fig. 7. Fluid density distributions with different rough morphologies.

secondary oscillation inside the grooves demonstrates an increasing trend as shown in Fig. 7(b). However, the density in mainstream region of the channel first decreases and then increases slightly. Obviously, the nanostructure free shear ratio has a more important influence on the density distribution of fluid.

Similarly, in the case of weak wall-fluid interaction, the variations of local relative surface friction coefficient with nanostructure free shear ratio and nanostructure morphology period are also discussed. Since the velocity profile in channel does not change along the flow direction as shown in Fig. 3, the local velocity gradient at the wall is basically unchanged. As a result, the local relative surface friction coefficients in both smooth and rough channel also remain invariable along the flow direction, as exhibited in Fig. 8. However, the local relative surface friction coefficient significantly depends on the wall rough morphology. As shown in Fig. 8(a), the average value of the local relative surface friction coefficient in channel increases with the augment of the nanostructure free shear ratio. Under the same nanostructure free shear ratio, the average value of the relative surface friction coefficient increases as the nanostructure depth increases. In comparison, as shown in Fig. 8(b), the average value of the local relative surface friction coefficient decreases with the augment of the nanostructure morphology period. Under the condition of the same nanostructure morphology period, with the augment of the nanostructure morphology depth, the average value of the relative surface friction coefficient also increases. Compared with smooth channel, the relative surface friction coefficients of rough channel increase dramatically. Physically, all these phenomena arise from the roughness effect on the local velocity gradient at the wall.

For visualization purposes, variations of the local velocity gradient in rough channel under different nanostructure free shear ratios are illustrated by velocity contours as shown in Fig. 9. To be consistent with the simulation parameters of the relative surface friction coefficient in Fig. 8 (a), the wall-fluid interaction of $\varepsilon_{sl}/\varepsilon_l = 0.25$ is chosen for depiction. As nanostructure free shear ratio varies from 0.1875 to 0.75, the maximum velocity at the center of the channel decreases gradually. Compared Fig. 9(a) and (b), under the same nanostructure free shear ratio, the larger the nanostructure depth, the lower the velocity in mainstream region of the channel. The decrease of the velocity in mainstream region of channel essentially depends on nanostructure roughness effect on the fluid velocity near the wall. Attributed to the larger nanostructure free shear ratio and nanostructure depth, the corresponding velocity slip is smaller and local velocity gradient at the wall is higher. Thus, the relative surface friction coefficient increases with the augments of the nanostructure free shear ratio and nanostructure depth.

4.4. Variation of local heat transfer characteristics

Fig. 10 shows the influence of rough nanostructure morphology on the local Nusselt number under the condition of weak wall-fluid interaction. The local Nusselt number gradually tends to be constant along the flow direction. It indicates that the heat transfer between the solid wall and the fluid gradually reaches a steady status. Different from the macroscale flow, the fluid temperature near nanochannel outlet is greatly affected by atoms of inlet hot fluid, which is attributed to the axial heat conduction derived from the periodic boundary condition [20–22,40]. Consequently, it leads to the fluctuation of local Nusselt number near the outlet, even a slight increase in variation of local Nusselt number near the outlet (Fig. 10(d)). By comparing Fig. 10(a) and (b), as well as Fig. 10(c) and (d), under the same rough nanostructure morphology, the larger the nanostructure depth, the greater the local Nusselt number. Moreover, the local Nusselt number in rough channel is also greater than that in smooth channel, which indicates that rough nanostructure morphology is conducive to heat transfer between solid wall and fluid.

4.5. Role of rough morphology in heat transfer and flow resistance

In order to analyze the influence of rough morphology on heat transfer and flow resistance better, the Nusselt number and flow resistance are discussed when the velocity and temperature distributions are fully developed. Fig. 11 shows the variations of thermal parameters in channel with weak wall-fluid interaction. Compared with the smooth channel (highlighted with a dashed box), the rough channel has a lower temperature jump at the wall-fluid interface due to the existence of nanostructure, which makes the Nusselt number in rough channel dramatically become greater. Obviously, the interfacial temperature jump is the main factor that influences heat transfer performance. In accordance with the other results [40,41], rough nanostructure could accommodate more fluid atoms within the grooves, which is beneficial for the reduction of temperature jump and facilitating the heat exchange between wall and fluid atoms. With the augments of nanostructure free shear ratio (Fig. 11 (a)) and nanostructure morphology period (Fig. 11 (b)), the temperature jump almost increases while the Nusselt number in rough channel decreases.

Fig. 12 intuitively demonstrates the effects of various rough morphologies and nanostructure depths on the Nusselt number. It is clear that Nusselt number corresponding to $h = 16$ Å is greater than that corresponding to $h = 4$ Å under the same rough morphology, which indicates that heat transfer between solid wall and fluid is enhanced by the augment of nanostructure depth. Yet, the Nusselt number has the same variation trend in both cases of $h = 16$ Å and $h = 4$ Å. In particular,

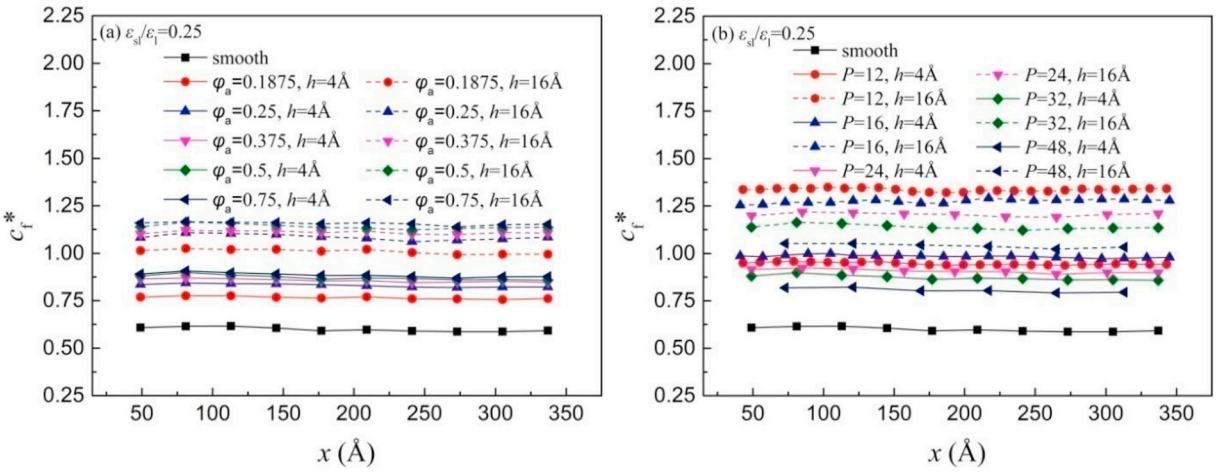

Fig. 8. Variation of the local relative surface friction coefficient along the channel.

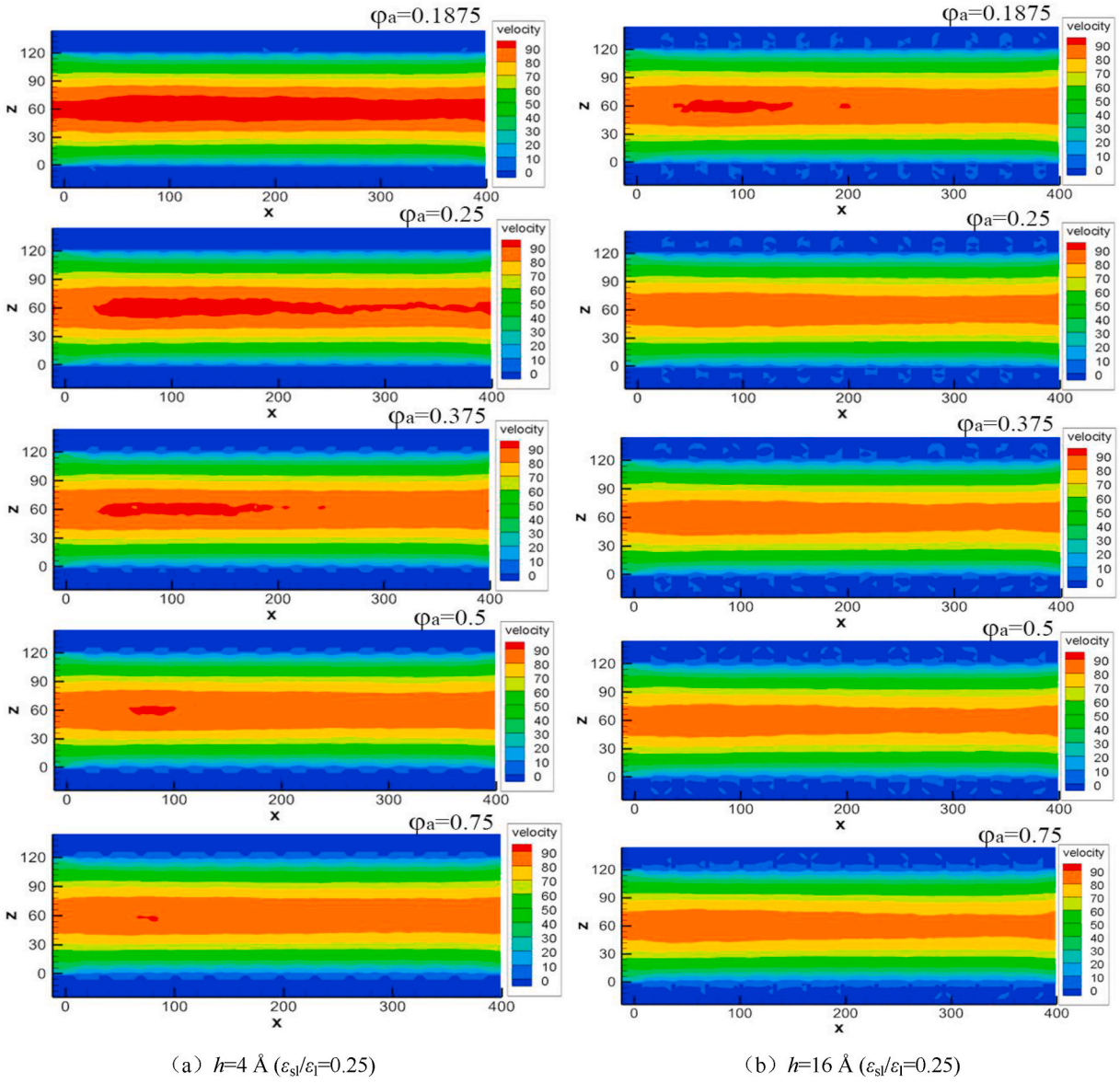

Fig. 9. Fluid velocity contours in rough channel.

the Nusselt number has a maximum when the nanostructure free shear ratio is $\phi_a = 0.1875$. Similarly, it has a maximum when the nanostructure morphology period is $P = 12$.

Fig. 13 and Fig. 14 show the influences of different rough nanostructure morphologies on the resistance coefficient of fully developed flow under the condition of weak wall-fluid interaction. For better comparison, a dashed line marked in pink is inserted in Figs. 13 and 14 to guide the eye, which represents the relative resistance coefficient in smooth channel under the strong wall-fluid interaction ($\varepsilon_{sl}/\varepsilon_l = 1.0$), where $f^* = 1.0$. Compared with the parameters in smooth channel (highlighted with a dashed box), the relative resistance coefficient and relative surface friction coefficient in rough channel are higher due to the wall roughness. As shown in Fig. 13, with the increase of nanostructure free shear ratio, the relative resistance coefficient and relative surface friction coefficient in rough channel increase gradually, which are derived from the reduction of interfacial velocity slip. In comparison, as the nanostructure morphology period increases shown in Fig. 14, the slip length increases while the relative resistance coefficient and the relative surface friction coefficient decrease gradually. As shown in Figs. 13 and 14, although the variation trends of resistance coefficient with rough morphology are similar in both cases of $h = 16$ Å and $h = 4$ Å, it is worth mentioning that the relative resistance coefficient and relative surface friction coefficient corresponding to the nanostructure depth of 4 Å are almost below the guide line of $f^* = 1.0$. The relative resistance coefficient and the relative surface friction coefficient corresponding to the nanostructure depth of 16 Å increase significantly, which are even higher (over the guide line of $f^* = 1.0$) than that in smooth channel with strong wall-fluid interaction.

Just as presented directly in Fig. 15, the relative resistance coefficient and relative surface friction coefficient corresponding to the nanostructure depth of 16 Å are greater compared with those corresponding to the nanostructure depth of 4 Å. However, in the cases of $h = 16$ Å and $h = 4$ Å, both the relative resistance coefficient and the relative surface friction coefficient have a minimum at $\phi_a = 0.1875$. Moreover, the relative resistance coefficient and the relative surface friction coefficient have a minimum at $P = 48$ as well. According to Figs. 12 and 15, it's found that the increase of nanostructure depth not only improves the heat transfer performance, but also greatly increases the flow resistance. Therefore, large nanostructure depth is not conducive to the drag reduction in rough channel.

Table 3 and Table 4 quantitatively show the influence of rough nanostructure morphology on the Nusselt number and resistance

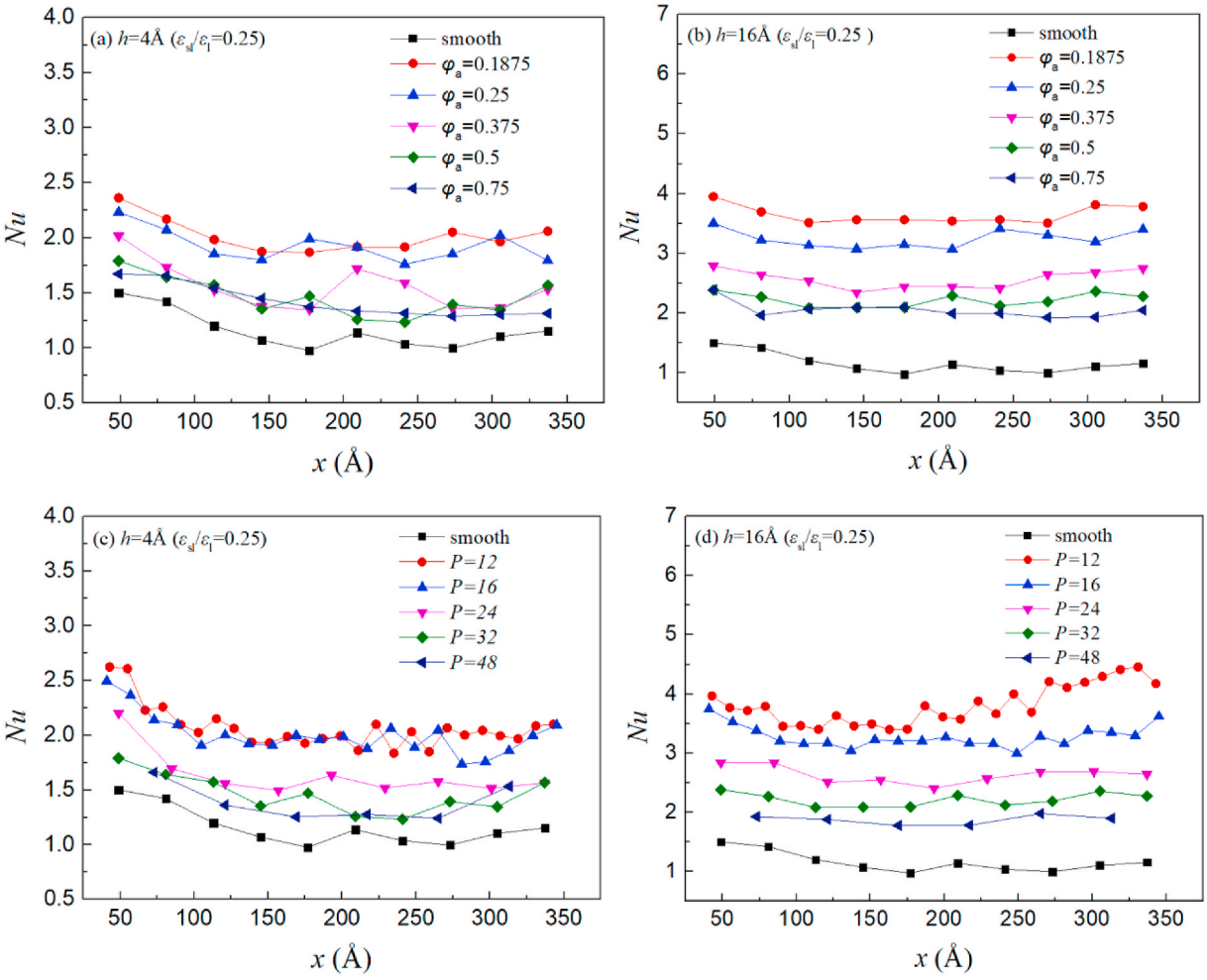

Fig. 10. Variation of local Nusselt number under different nanostructure morphologies.

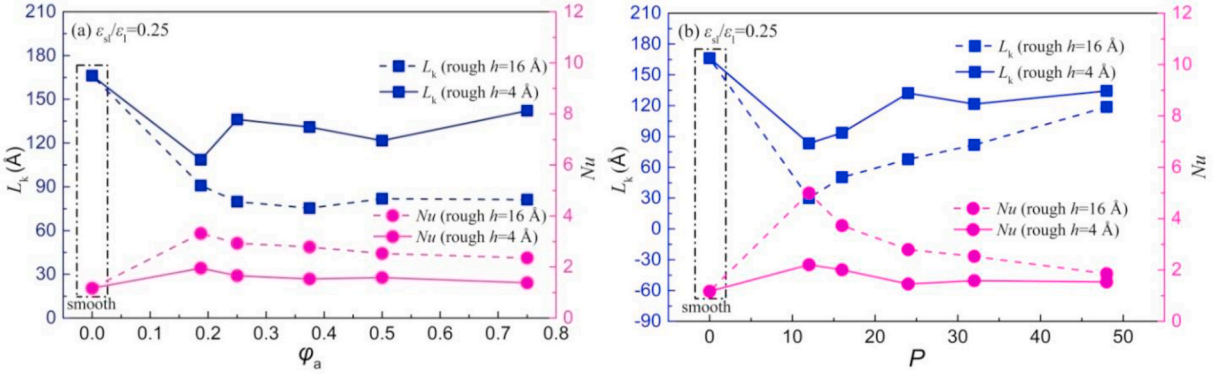

Fig. 11. Variation of heat transfer characteristic with different nanostructure morphologies.

coefficient in channel under the condition of the weak wall-fluid interaction. Here, the variation rates of all parameters are obtained based on the corresponding values of smooth channel with the strong wall-fluid interaction. As shown in Table 3 and Table 4, the Nusselt number of rough channel with nanostructure depth of 16 Å is greatly increased, while its corresponding relative resistance coefficient is also mostly increased and the drag reduction characteristics becomes weak. However, the relative resistance coefficients in both smooth channel and rough channel with nanostructure depth of 4 Å decrease, which indicates that both cases have better drag reduction characteristics. Yet, the decrease rate of Nusselt number in rough channel with nanostructure depth of 4 Å is much lower than that in smooth channel. Furthermore, the Nusselt number corresponding to the nanostructure depth of 4 Å is more close to the Nusselt number in smooth channel with the strong wall-fluid interaction. In particular, when the nanostructure free shear ratio is $\varphi_a = 0.1875$, the Nusselt number corresponding to the nanostructure depth of 4 Å only decreases by 1.8%, but the maximum decrease rates of the relative resistance coefficient and relative surface friction coefficient are 27.1% and 25.3%, respectively. The heat transfer performance and drag reduction characteristics are the best at $\varphi_a =$

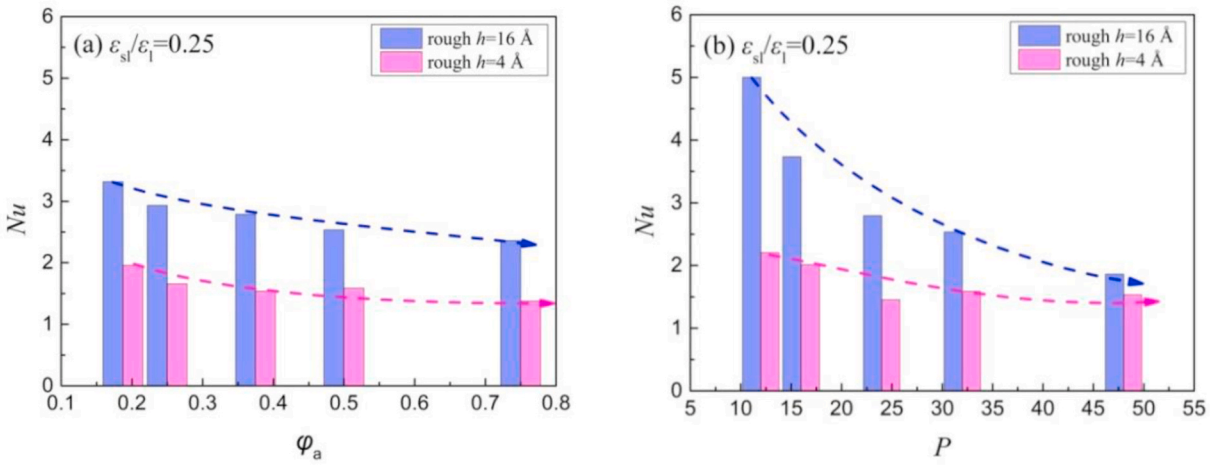

Fig. 12. Variation of fully-developed Nusselt number under different nanostructure morphologies.

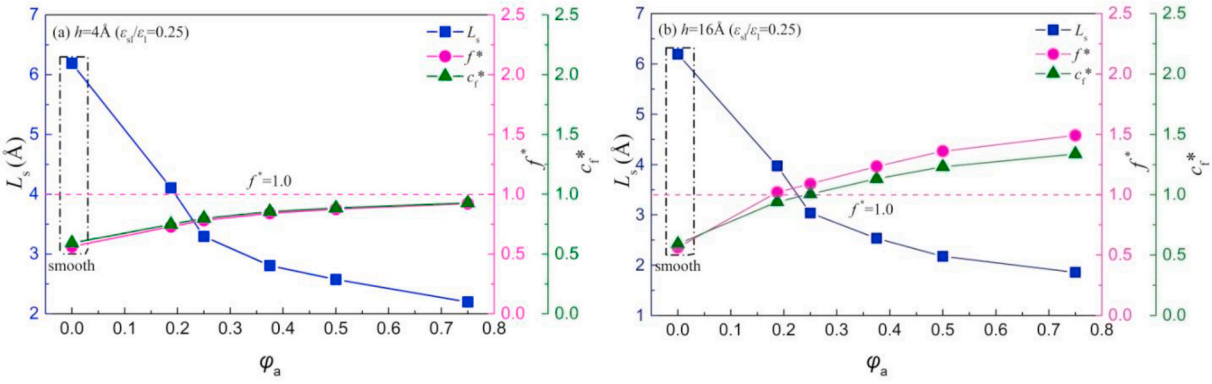

Fig. 13. Variation of flow resistance under different nanostructure free shear ratios.

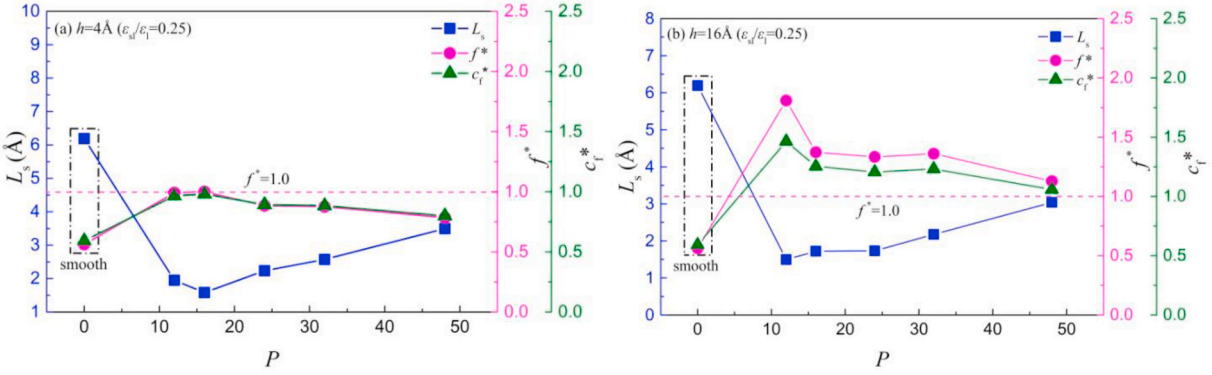

Fig. 14. Variation of flow resistance under different nanostructure morphology periods.

0.1875. With the increase of the nanostructure free shear ratio, the nanostructure width increases and the nanostructure spacing decreases, both the drag reduction characteristics and heat transfer efficiency are weakened.

As shown in Table 4, when the nanostructure morphology period is $P = 48$, the Nusselt number corresponding to the nanostructure depth of 4 Å decreases by 22.9%, the maximum decrease rate of relative resistance coefficient and relative surface friction coefficient are 21.5% and 20.1%, respectively. The rough channel with the nanostructure morphology period of 48 Å has the best drag reduction characteristics, and the Nusselt number is significantly greater than that in the smooth channel (with the greater decrease rate of 41.3%). As the nanostructure morphology period decreases, the number of nanostructure grooves increases, the rough morphology of the channel wall becomes dense, the heat transfer performance is improved while the flow resistance becomes greater gradually.

Obviously, the heat transfer and flow resistance in rough channel are greatly related to the nanostructure free shear ratio (width, spacing), nanostructure depth, and nanostructure morphology period (groove number). The Nusselt number decreases with the augments of nanostructure free shear ratio and nanostructure morphology period. The relative resistance coefficient increases with the augment of the nano-

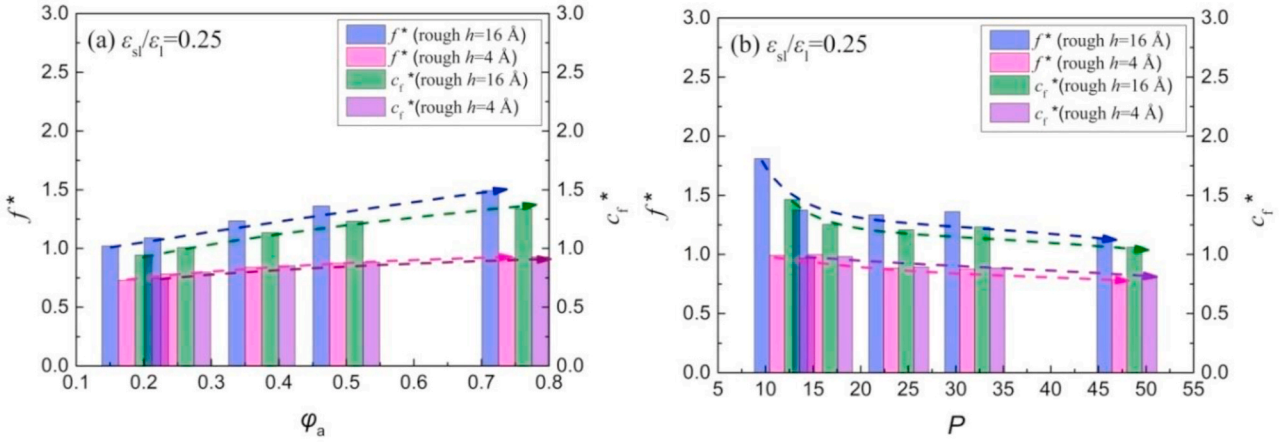

Fig. 15. Variation of resistance coefficient under different rough nanostructure morphologies.

Table 3
Variation rates of Nusselt number and resistance coefficient under different nanostructure free shear ratios.

Nanostructure depth	Parameters	$\varphi_a(\varepsilon_{sl}/\varepsilon_l = 0.25)$					
		0 (smooth)	0.1875	0.25	0.375	0.5	0.75
h = 4 Å	Nu	41.3%↓	1.8%↓	16.8%↓	22.9%↓	20.4%↓	30.7%↓
	f^*	43.7%↓	27.1%↓	21.8%↓	15.9%↓	12.4%↓	7.8%↓
	cf^*	40.9%↓	25.3%↓	20.2%↓	14.6%↓	11.5%↓	7.2%↓
h = 16 Å	Nu	41.3%↓	66.4%↑	47.2%↑	39.9%↑	27.3%↑	18.5↑
	f^*	43.7%↓	2.1%↑	8.9%↑	23.5%↑	36.2%↑	49.2%↑
	cf^*	40.9%↓	5.7%↓	0.7%↑	13.3%↑	23.1%↑	33.7%↑

Table 4
Variation rates of Nusselt number and resistance coefficient under different nanostructure morphology periods.

Nanostructure depth	Parameters	P ($\varepsilon_{sl}/\varepsilon_l = 0.25$)					
		0 (smooth)	12	16	24	32	48
h = 4 Å	Nu	41.3%↓	10.6%↑	0.9%↑	27.0%↓	20.4%↓	22.9%↓
	f^*	43.7%↓	0.9↓	0.03%↓	11.6%↓	12.4%↓	21.5%↓
	cf^*	40.9%↓	3.3%↓	1.8%↓	10.7%↓	11.5%↓	20.1%↓
h = 16 Å	Nu	41.3%↓	151.1%↑	87.5%↑	40.2%↑	27.3%↑	6.7↓
	f^*	43.7%↓	80.9%↑	37.4%↑	33.4%↑	36.2%↑	12.9%↑
	cf^*	40.9%↓	46.4%↑	25.3%↑	20.7%↑	23.1%↑	5.9%↑

structure free shear ratio, while decreases with the augment of the nanostructure morphology period. The rough channel with nanostructure depth of 4 Å can not only enhance heat transfer, but also obtain a considerable drag reduction. Therefore, the nanostructure free shear ratio with $\phi_a = 0.1875$ is a favorable rough morphology to obtain optimum convective heat transfer performance in present considered nanochannel.

5. Conclusions

Based on the molecular dynamics theory, a three-dimensional model of convective heat transfer in parallel plate nanochannel with constant wall temperature is established. The distributions of fluid velocity, temperature and density in rough channel are discussed. Under the weak wall-fluid interaction, the effects of nanostructure free shear ratio, nanostructure morphology period and nanostructure depth on the heat transfer performance and flow resistance characteristics are analyzed. The conclusions are drawn as following:

(1) The wall-fluid interaction and rough morphology have an important influence on the heat transfer and flow resistance characteristics. Compared with the smooth channel, the corresponding rough channel with the weak wall-fluid interaction not only has considerable drag reduction, but also has better heat transfer performance.
(2) The smaller the nanostructure free shear ratio, the better heat transfer performance as well as drag reduction characteristics. The smaller the nanostructure morphology period, the better the heat transfer performance, but the weaker the drag reduction characteristics. By evaluating the heat transfer and flow characteristics comprehensively, the nanostructure free shear ratio with $\phi_a = 0.1875$ is a most favorable rough morphology to obtain optimum heat transfer performance.
(3) The larger the rough nanostructure depth, the better the heat transfer between fluid and channel wall, but the greater the flow resistance. Thus, a smaller nanostructure depth is more conducive to achieve better heat transfer performance and drag reduction simultaneously.

Declaration of competing interest

The authors declare that they have no known competing financial interests or personal relationships that could have appeared to influence the work reported in this paper.

Data availability

The data that has been used is confidential.

Acknowledgment

The authors gratefully acknowledge the financial support by the Key Natural Science Foundation of Tianjin (No.17JCZDJC31200).

References

[1] O. Mahian, L. Kolsi, M. Amani, P. Estellé, et al., Recent advances in modeling and simulation of nanofluid flows—Part II: Applications, Phys. Rep. 791 (2019) 1–59.
[2] H.Y. Sun, F. Li, M. Wang, G.M. Xin, X.Y. Wang, Molecular dynamics study of convective heat transfer mechanism in a nano heat exchanger, RSC Adv. 10 (2020) 23097.
[3] Z.Y. Guo, Z.X. Li, Size effect on microscale single-phase flow and heat transfer, Int. J. Heat Mass Tran. 46 (2003) 149.
[4] S.W. Zhang, F. Hao, H.M. Chen, W. Yuan, Y. Tang, X. Chen, Molecular dynamics simulation on explosive boiling of liquid argon film on copper nanochannels, Appl. Therm. Eng. 113 (2017) 208–214.
[5] H. Hu, Y. Sun, Effect of nanopatterns on Kapitza resistance at a water-gold interface during boiling: a molecular dynamics study, J. Appl. Phys. 112 (5) (2012), 053508.
[6] A. Pham, M. Barisik, B. Kim, Pressure dependence of Kapitza resistance at gold/water and silicon/water interfaces, J. Chem. Phys. 139 (24) (2013) 244702.
[7] M. Barisik, A. Beskok, Temperature dependence of thermal resistance at the water/silicon interface, Int. J. Therm. Sci. 77 (2014) 47–54.
[8] C. Liu, H.B. Fan, K. Zhang, Matthew M.F. Yuen, Z.G. Li, Flow dependence of interfacial thermal resistance in nanochannels, J. Chem. Phys. 132 (9) (2010), 094703.
[9] W. Wang, S. Huang, X. Luo, MD simulation on nano-scale heat transfer mechanism of sub-cooled boiling on nano-structured surface, Int. J. Heat Mass Tran. 100 (2016) 276–286.
[10] Y.H. Wang, S.Y. Wang, G. Lu, X.D. Wang, Explosive boiling of nanoliquid argon films on high temperature platinum walls: effects of surface wettability and film thickness, Int. J. Therm. Sci. 132 (2018) 610–617.
[11] F.C. Wang, Y.P. Zhao, Slip boundary conditions based on molecular kinetic theory: the critical shear stress and the energy dissipation at the liquid-solid interface, Soft Matter 7 (18) (2011) 8628–8634.
[12] W. Gao, X. Zhang, X.T. Han, C.Q. Shen, Role of solid wall properties in the interface slip of liquid in nanochannels, Micromachines 9 (12) (2018) 663.
[13] P. Alipour, et al., Modeling different structures in perturbed Poiseuille flow in a nanochannel by using of molecular dynamics simulation: study the equilibrium, Phys. Stat. Mech. Appl. 515 (2019) 13–30.
[14] M. Jeong, Y. Kim, W.J. Zhou, W.Q. Tao, M.Y. Ha, Effects of interface wettability, roughness and moving wall velocity on the Couette flow in nanochannel using multi-scale hybrid method, Comput. Fluids 147 (2017) 1–11.
[15] H. Rahmatipour, A. Azimian, O. Atlaschian, Study of fluid flow behavior in smooth and rough nanochannels through oscillatory wall by molecular dynamics simulation, Phys. Stat. Mech. Appl. 465 (2017) 159–174.
[16] C. Jiang, O. Jie, L. Wang, Q. Liu, X. Wang, Transport properties and structure of dense methane fluid in the rough nano-channels using non-equilibrium multiscale molecular dynamics simulation, Int. J. Heat Mass Tran. 110 (2017) 80–93.
[17] A. Loya, J.L. Stair, A.R. Jafri, K. Yang, G. Ren, A molecular dynamic investigation of viscosity and diffusion coefficient of nanoclusters in hydrocarbon fluids, Comput. Mater. Sci. 99 (2015) 242–246.
[18] A.E. Giannakopoulos, F. Sofos, T.E. Karakasidis, A. Liakopoulos, Unified description of size effects of transport properties of liquids flowing in nanochannels, Int. J. Heat Mass Tran. 55 (19–20) (2012) 5087–5092.
[19] A.J. Markvoort, P. Hilbers, S. Nedea, Molecular dynamics study of the influence of wall-gas interactions on heat flow in nanochannels, Phys. Rev. 71 (6) (2005), 066702.
[20] S. Ge, Y. Gu, M. Chen, A molecular dynamics simulation on the convective heat transfer in nanochannels, Mol. Phys. 113 (7) (2015) 703–710.
[21] Y.W. Gu, S. Ge, M. Chen, A molecular dynamics simulation of nanoscale convective heat transfer with the effect of axial heat conduction, Mol. Phys. 114 (12) (2016) 1922–1930.
[22] D.C. Marable, S. Shin, A. YousefzadiNobakht, Investigation into the microscopic mechanisms influencing convective heat transfer of water flow in graphene nanochannels, Int. J. Heat Mass Tran. 109 (2017) 28–39.
[23] T.M. Thomas, N. Vinod, Convective heat transfer between liquid argon flows and heated carbon nanotube Arrays using molecular dynamics, J. Appl. Fluid Mech. 12 (3) (2019) 971–980.
[24] P. Keblinski, S.R. Phillpot, S.U.S. Choi, et al., Mechanisms of heat flow in suspensions of nano-sized particles (nanofluids), Int. J. Heat Mass Tran. 45 (4) (2002) 855–863.
[25] J.A. Eastman, S.R. Phillpot, S.U.S. Choi, et al., Thermal transport in nanofluids, Annu. Rev. Mater. Res. 34 (2004) 219–246.
[26] A. Arshad, M. Jabbal, Y. Yan, D. Reay, A Review on graphene based nanofluids: preparation, characterization and applications, J. Mol. Liq. 279 (2019) 444–484.
[27] J. Buongiorno, D.C. Venerus, N. Prabhat, et al., A benchmark study on the thermal conductivity of nanofluids, J. Appl. Phys. 106 (2009), 094312.
[28] S.A. Angayarkanni, J. Philip, Review on thermal properties of nanofluids: recent developments, Adv. Colloid Interface Sci. 225 (2015) 146–176.
[29] S.A. Angayarkanni, V. Sunny, J. Philip, Effect of nanoparticle size, morphology and concentration on specific heat capacity and thermal conductivity of nanofluids, Journal of Nanofluids 4 (2015) 302–309.
[30] A.K. Mishra, B.B. Lahiri, J. Philip, Thermal conductivity enhancement in organic phase change material (phenol-water system) upon addition of Al_2O_3, SiO_2 and TiO_2 nanoinclusions, J. Mol. Liq. 269 (2018) 47–63.
[31] A.K. Mishra, B.B. Lahiri, J. Philip, Effect of surface functionalization and physical properties of nanoinclusions on thermal conductivity enhancement in an organic phase change material, ACS Omega 3 (2018) 9487–9504.
[32] M.B. Motlagh, M. Kalteh, Simulating the convective heat transfer of nanofluid Poiseuille flow in a nanochannel by molecular dynamics method, Int. Commun. Heat Mass Tran. 111 (2020) 104478.
[33] M.B. Motlagh, M. Kalteh, Molecular dynamics simulation of nanofluid convective heat transfer in a nanochannel: effect of nanoparticles shape, aggregation and wall roughness, J. Mol. Liq. 318 (2020) 114028.
[34] P.F. Xu, Q. Li, Y.M. Xuan, Enhanced boiling heat transfer on composite porous surface, Int. J. Heat Mass Tran. 80 (2015) 107–114.
[35] Y.Q. Wang, J.L. Luo, Y. Heng, D.C. Mo, S.S. Lyu, Wettability modification to further enhance the pool boiling performance of the micro nano bi-porous copper surface structure, Int. J. Heat Mass Tran. 119 (2018) 333–342.
[36] G. Liang, Y. Chen, H. Yang, D. Li, S. Shen, Nucleate boiling heat transfer and critical heat flux (CHF) from micro-pit surfaces, Int. J. Heat Mass Tran. 152 (2020) 119510.
[37] S. Xie, M. Jiang, H. Kong, Q. Tong, J. Zhao, An experimental investigation on the pool boiling of multi-orientated hierarchical structured surfaces, Int. J. Heat Mass Tran. 164 (2021) 120595.
[38] S. Xie, Q. Tong, Y. Guo, X. Li, H. Kong, J. Zhao, The effects of surface orientation, heater size, wettability, and subcooling on the critical heat flux enhancement in pool boiling, Int. J. Heat Mass Tran. 149 (2020) 119230.
[39] B.Y. Cao, M. Chen, Z.Y. Guo, Effect of surface roughness on gas flow in microchannels by molecular dynamics simulation, Int. J. Eng. Sci. 44 (2006) 927–937.
[40] P. Chakraborty, T.F. Ma, L. Cao, Y. Wang, Significantly enhanced convective heat transfer through surface modification in nanochannels, Int. J. Heat Mass Tran. 136 (2019) 702–708.
[41] M.B. Motlagh, M. Kalteh, Investigating the wall effect on convective heat transfer in a nanochannel by molecular dynamics simulation, Int. J. Therm. Sci. 156 (2020) 106472.
[42] S. Yao, J. Wang, X. Liu, The influence of wall properties on convective heat transfer in isothermal nanochannel, J. Mol. Liq. 324 (2021) 115100.
[43] B. Wang, J.D. Wang, Z.L. Dou, et al., Investigation of retention of gases in transverse hydrophobic microgrooved surfaces for drag reduction, Ocean Eng. 79 (2014) 58–66.
[44] B.R.K. Gruncell, N.D. Sandham, G. Mchale, Simulations of laminar flow past a super hydrophobic sphere with drag reduction and separation delay, Phys. Fluids 25 (4) (2013), 043601.
[45] M.A. Samaha, H.V. Tafreshi, M. Gad-El-Hak, Modeling drag reduction and meniscus stability of superhydrophobic surfaces comprised of random roughness, Phys. Fluids 23 (1) (2011), 012001.
[46] E. Aljallis, M.A. Sarshar, R. Datla, et al., Experimental study of skin friction drag reduction on superhydrophobic flat plates in high Reynolds number boundary layer flow, Phys. Fluids 25 (2) (2013), 025103-025114.
[47] H. Park, H. Park, J. Kim, A numerical study of the effects of super hydrophobic surface on skin-friction drag in turbulent channel flow, Phys. Fluids 25 (11) (2013) 110815.
[48] S. Plimpton, Fast parallel algorithms for short-range molecular dynamics, Journal of Computer Physics 117 (1) (1993) 1–19.
[49] D. Toghraie, M. Mokhtari, M. Afrand, Molecular dynamic simulation of copper and platinum nanoparticles Poiseuille flow in a nanochannel, Physica E 84 (2016) 152–161.
[50] K.K. Kammara, G. Malaikannan, R. Kumar, Molecular dynamics study of gas–surface interactions in a force-driven flow of argon through a rectangular nanochannel, Nanoscale Microscale Thermophys. Eng. 20 (2) (2016) 121–136.
[51] S.T. Yao, J.S. Wang, X.L. Liu, Y. Jiao, The effects of surface topography and non-uniform wettability on fluid flow and interface slip in rough nanochannel, J. Mol. Liq. 301 (2020) 112460.
[52] P.G. Gennes, Wetting statics and dynamics, Rev. Mod. Phys. 57 (3) (1985) 827–863.
[53] W.D. Wang, H.Y. Zhang, C.H. Tian, X.J. Meng, Numerical experiments on evaporation and explosive boiling of ultra-thin liquid argon film on aluminum nanostructure substrate, Nanoscale Research Letters 10 (2015) 158.
[54] B. Shi, Vijay K. Dhir, Molecular dynamics simulation of the contact angle of liquids on solid surfaces, J. Chem. Phys. 130 (2009), 034705.
[55] N. Asproulis, D. Drikakis, Surface roughness effects in micro and nanofluidic devices, J. Comput. Theor. Nanosci. 7 (9) (2010) 1825–1830.